STATIC RESPONSE OF COATED MICROBUBBLES: MODELLING SIMULATIONS AND PARAMETER ESTIMATION

Alkmini D. Lytra[1], Nikos A. Pelekasis[1], Vassiliki I. Zafiropoulou[2], Thanasis Zisis[3], Antonios E. Giannakopoulos[2], Vassilis Sboros[4], Emmanouil Glynos[5] and Vasileios Koutsos[6]

[1]Department of Mechanical Engineering
University of Thessaly
Volos, GR-38334, Greece
e-mail: pel@uth.gr ; web page:
http://www.mie.uth.gr

[2]Department of Civil Engineering
University of Thessaly
Volos, GR-38334, Greece

[3]Department of Applied Mathematical & Physical Sciences
National Technical University of Athens
Athens, GR-15773, Greece

[4]School of Engineering & Physical Sciences
Heriot Watt University
Edinburgh, EH14, 4AS, United Kingdom

[5]Department of Materials Science & Engineering, Biointerfaces Institute
University of Michigan
Ann Arbor, 48109, United States of America

[6]Institute for Materials & Processes, School of Engineering
University of Edinburgh
Edinburgh, EH 9JL, United Kingdom

Keywords: Stretching, Bending, Gas Compressibility, Shell Thickness, Area Dilatation, Bending Modulus.

Abstract. *We present a methodology in order to estimate the elastic properties of contrast agent microbubbles by employing asymptotic relations from classical shell theory and an extension for plane contact. The estimated values are in agreement with experimental (AFM) values for polymeric shells. Moreover, a numerical (FEM) model aims at the description of static response of contrast agents in order to reveal the main mechanisms that deform the elastic shell when it is compressed by the AFM. Simulations with Abaqus corroborate the static pre- and post-buckling behavior identified by simple point load calculations. Finally, simulations that account for the load distribution and include surface adhesion effects are performed in order to verify the importance of elastocapillarity at very small deformations and provide an alternative parameter estimation procedure for soft phospholipid shells.*

1 INTRODUCTION

Contrast agents (CA) are microbubbles covered with an elastic shell, usually made of polymeric or lipid biomaterials providing mechanical strength and decelerating the gas dissolution in vivo [1]. Their initial diameter ranges from 3 to5 μm and their thickness from 10 to 40 nm [2]-[4]. CA microbubbles have been successfully used during the last decades for imaging human organs and they are considered as drug/gene carriers for therapeutic application of diseases [5], [6]. In both cases the elastic properties of the shell are key parameters that control their behavior when exposed to ultrasound and as they travel through the vascular bed. The present work aims at the estimation of the Young's and bending modulus of shell coatings by employing finite elements, experimental data and asymptotic analysis.

In particular, Glynos et al. [3] have investigated the mechanical response of CA microbubbles covered with polymeric material by employing the atomic force microscope (AFM), which can accurately measure the force and the resultant deformation. Polymers are considered as harder shells comparing to lipids, in terms of their Young's modulus. They consist of a stiff polylactide shell surrounded by a thin (~10 nm) layer of cross-linked albumin outer layer to make microbubbles harmless to the human body. An extensive number of force-deformation curves (to be referred to as f-d in the following for brevity) can be found in the work of Glynos et al [3] by using various cantilever stiffness (k_c). Four different regimes were observed in the f-d curves, see Figure 1(a). The f-d curves exhibit an initial short nonlinear [7], [8] [9] regime up to about 10 nm and 10 nN pertaining to interfacial forces between the cross-linked albumin outer layer and the cantilever, denoted with 1 in Figure 1(a). Then an extensive linear regime (denoted with 2 and known as Reissner regime) is observed where the elastic forces originating from the stiff polylactide layer are dominant [10]. The linear regime is followed by a

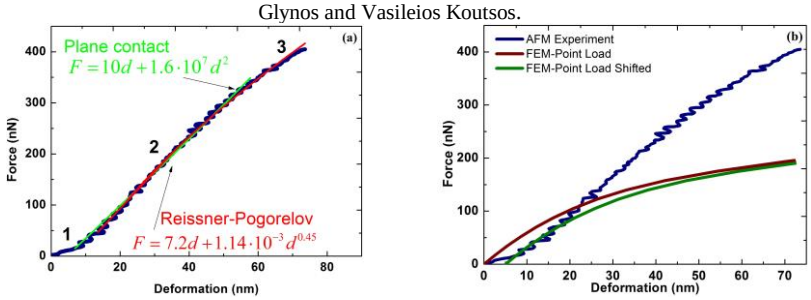

Figure 1 (a) Asymptotic fitting in f-d curve of a polymeric microbubble [3], (b) Comparison between experimental [3] and FEM results for a point load on a polymeric microbubble

nonlinear [11], [12], but curved downwards regime, also known as Pogorelov regime (3). Finally, at large enough deformations the f-d curve exhibit a fourth regime which is slightly curved upwards, indicating the effect of gas compressibility on the composite stiffness of the microbubble [13]. This regime becomes mostly evident when soft phospholipid shells are examined by the AFM [2], see also the discussion in section 3.2. Combining the above regimes and employing asymptotic relations available from literature [10], [11] allows for the estimation of Young's modulus (E) and shell thickness (h) [13]. When phospholipids are examined with the AFM the response registered in f-d curves differs significantly. In particular, the range of applied forces is ten times smaller in comparison with polymeric shells and it is in the range of intermolecular forces. As a result the latter contribute on the force balance thus modifying or even bypassing translation from Reissner to Pogorelov regime and new asymptotic relations are necessary in order to estimate their elastic properties.

As can be gleaned from the AFM experiment [2]-[4], the shell is compressed by a static load while in contact with a plane and stiff cantilever. Therefore, in order to simulate the above experiment we introduce the non-linear equations of continuum shell mechanics and we employ the finite element methodology in order to estimate its deformation. Moreover, the microbubble core consists of a gas (usually nitrogen), which is initially at atmospheric (ambient) pressure, but its volume decreases while the shell is compressed. Consequently, the ideal gas law for isothermal compression is introduced in order to estimate the internal gas pressure. Another aspect that we wish to investigate numerically, that is essential for phospholipids, is the effect of interfacial forces between different surfaces in contact, e.g. microbubble-cantilever and microbubble water. In the same context, it is important to explain the effect of the contact pressure distribution in f-d curves, in order to build new tools of experimental assessment. Further discussion on the theoretical analysis can be found in section 2. The main results and conclusions of the present investigation are in sections 3 and 4, respectively.

2 PROBLEM FORMULATION

2.1 Theoretical Modeling

The elastic shell is considered to follow axisymmetric deformations, Figure 2(a) – (c), and it is discretized by Lagrangian particles (ξ). The initial and final position of every particle ξ can be described by the following normal $\vec{n}$ and tangential $\vec{t}_s, \vec{t}_\varphi$ vectors on the shell surface [14].

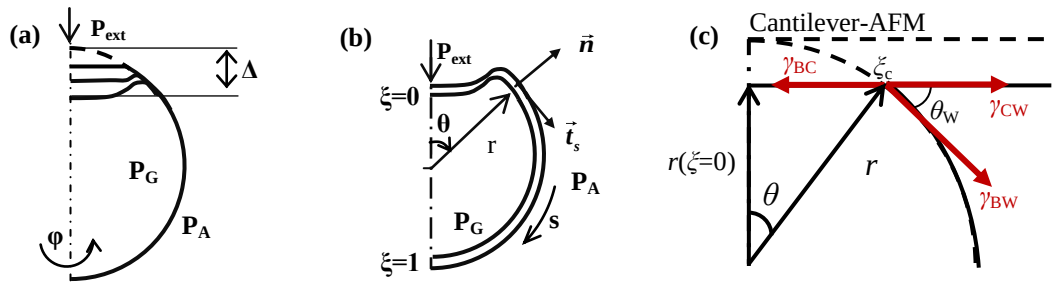

Figure 2. (a) Deformed bubble subject to an increasing static point load, (b) lagrangian representation, (c) schematic description of contact between the microbubble and the AFM

In order to simulate the behavior of microbubbles subject to a static load, as is the case in AFM experiment measurements, the normal and tangential force balance are employed, written in spherical axisymmetric form [13, 15-19],

$$\Delta\vec{F} = \Delta F_n\vec{n} + \Delta F_s\vec{t}_s = -\vec{\nabla}_s\cdot\left[\underline{\underline{T}} + \gamma\left(\underline{\underline{I}} - \vec{n}\vec{n}\right)\right] = \Delta P\vec{n}$$

$$\underline{\underline{T}} = \underline{\underline{\tau}} + \vec{q}\vec{n}, \qquad \underline{\underline{\tau}} = \tau_s\vec{t}_s\vec{t}_s + \tau_\varphi\vec{t}_\varphi\vec{t}_\varphi, \qquad \vec{q} = q\vec{t}_s, \qquad \Delta P = \begin{cases} P_{ext} + P_A - P_G & ,\xi = 0 \\ P_A - P_G & ,\xi \neq 0 \end{cases} \tag{1}$$

where, ∇_s is the surface gradient operator, $\boldsymbol{T}$ is the tension tensor, which contains the in-plane ($\boldsymbol{\tau}$) and the shear ($\boldsymbol{qn}$) tension tensors and P_{ext}, P_A and P_G are the applied point load, the ambient and the gas pressure, respectively. Moreover, upon performing a torque balance on an infinitesimal shell patch, the shear $\boldsymbol{q}$ tension is related to the bending moment $\boldsymbol{m}$ tensor:

$$\vec{q} = \vec{\nabla}_s\cdot\underline{\underline{m}}\cdot\left(\underline{\underline{I}} - \vec{n}\vec{n}\right), \qquad \underline{\underline{m}} = m_s\vec{t}_s\vec{t}_s + m_\varphi\vec{t}_\varphi\vec{t}_\varphi, \qquad m_i = k_b\left(K_i + \nu K_j\right)/\lambda_j, \qquad K_i \equiv \lambda_i k_i - k_i^R \tag{2}$$

$$k_b = Eh^3/12\left(1-\nu^2\right), \qquad \lambda_i = ds_i/dS_i \quad i,\, j = s \text{ or } \varphi \quad i \neq j \text{ indices are not summed} \tag{3}$$

The gas that is encapsulated in the microbubble follows isothermal compression as its volume changes:

$$P_G V_f = P_A V_i \tag{4}$$

where indices *f* and *i* signify the microbubble volume (*V*) in the stress free and deformed stages, respectively. The formulation is completed with the appropriate boundary conditions of symmetry for *r* and θ variables at the two poles signified by Lagrangian particles ξ=0 and ξ=1.

$$r_\xi = 0 \quad \text{at} \quad \xi = 0 \quad \text{and} \quad \xi = 1, \qquad \textit{and} \qquad \theta_{\xi\xi\xi} = 0 \quad \text{at} \quad \xi = 0 \quad \text{and} \quad \xi = 1 \tag{5}$$

More details on the above formulation are provided in [13, 24]. Thus far it is assumed that the cantilever acts as a point load on the microbubble, an assumption that is strictly valid for small deformations. In order to properly simulate the contact between the AFM and the microbubble and the flattening of the shell, a kinematic constraint is considered [20] which allows the exact calculation of the pressure distribution at the contact area. The kinematic condition reads:

$$r\left(\xi = 0\right) = r\cos\theta \quad \text{for} \quad \xi \in \left[0, \xi_c\right] \tag{6}$$

where ξ_c signifies the Lagrangian particle at the end of contact line, Figure 2(c). In this case, the boundary conditions for the unknown pressure are:

$$P_{ext,\,\xi} = 0 \quad \text{at} \quad \xi = 0 \quad \text{and} \quad P_{ext,\,\xi} = L_\xi \quad \text{at} \quad \xi = \xi_c \tag{7a}$$

with L_ξ being an estimate of the first derivative at ξ=ξ_c based on Lagrange interpolation with the last four points [21] of the contact region. Moreover, when ξ=0, equation (10) becomes trivial and it is replaced by an estimation of the second derivative.

$$P_{ext,\,\xi\xi\xi} = L_{\xi\xi\xi} \quad \text{at} \quad \xi = 0 \tag{7b}$$

In this fashion the unknown vector (*r*, θ, P_G, P_{ext}) depends mainly on two dimensionless numbers:

$$\tilde{k}_b = \frac{k_b}{\chi R_o^2} = \left(\frac{h}{3R_0}\right)^2, \qquad \tilde{P} = \frac{P_A R_o}{\chi}, \qquad \chi \equiv Eh \tag{8}$$

with $\tilde{k}_b$ denoting the ratio of bending resistance over stretching and $\tilde{P}$ the ratio of resistance due to gas compressibility over stretching.

Currently the above formulation is extended in order to capture the effect of surface energy, Figure 2(c). In particular, the shell surface is divided into two domains, e.g. the contact area and the free shell, whereas two different B-cubic splines representations are considered. This approach introduces four additional coefficients for radial (*r*) and polar (θ) position of the particles, two of them at the end of the contact area and another two at the beginning of the free shell. Therefore, four more equations are required in order to balance the number of

unknowns. The first two enforce continuity of r and θ positions, calculated at the end of the contact area (ξ_c=1) and the beginning of the free shell (ξ=0):

$$r(\xi_c = 1) = r(\xi = 0) \quad \text{and} \quad \theta(\xi_c = 1) = \theta(\xi = 0) \tag{9}$$

while the other two constitute a force and a moment balance over the contact line:

$$(\tau_{ss} + \gamma)_{BC} = \gamma_{CW} + (\tau_{ss}\cos\theta_w + q\sin\theta_w + \gamma\cos\theta_w)_{BW} \tag{10}$$

$$(qr_c - m_{ss} - P_{ext}r_c)_{BC} = (qr_c\cos\theta_w - m_{ss} - \tau_{ss}r_c\sin\theta_w + \gamma r_c\sin\theta_w)_{BW} \tag{11}$$

where γ_{BC}, γ_{BW} and γ_{CW} signify the surface tension between bubble-cantilever, bubble-water and cantilever water, respectively. Moreover, θ_W is the wetting angle and r_c the contact length.

2.2 Finite Element Implementation

The normal and tangential force balances coupled with the isothermal ideal gas compression law and the kinematic condition, are discretized with the finite element methodology in order to capture the displaced Lagrangian particles (ξ) in terms of their spherical coordinates, r and θ, along the generating curve of the axisymmetric shell, the internal gas pressure and the load distribution (P_{ext}) in the contact area. The unknown Lagrangian particle positions and the pressure distribution are written as a function of a number of B-cubic spline polynomials [22]:

$$r(\xi) = \sum_{i=0}^{N+1} a_i B_i, \qquad \theta(\xi) = \sum_{i=0}^{N+1} b_i B_i \qquad \text{and} \qquad P_{ext}(\xi) = \sum_{i=0}^{M+1} c_i B_i \tag{12}$$

where N and M denote the number of nodes along the discretized domain and the contact area, respectively, and a_i, b_i, c_i are the unknown coefficients. The choice of B-cubic splines polynomials as basis function was based on the fact that fourth order derivatives of r and θ coordinates enter the force balance, due to bending terms. However, after integration by parts is performed the weak form of the normal and tangential force balances contains up to 2nd and 3rd order derivatives, respectively. Since cubic splines guarantee continuity up to the 2nd derivative [21-23] the above weak formulation is valid.

The solution of the above system of equations is obtained using an iterative scheme in a standard Newton's algorithm. The computational domain is typically discretized by 400 elements, while a finer mesh essentially reproduces the above result. An in house fortran code has been validated by calculating the critical buckling load and comparing the numerical value with the analytical expression for a uniform external load [13]. An extensive discussion of benchmark calculations pertaining to the static response of the microbubble subject to a point load can be found in previous work [24].

2.3 Asymptotic Analysis

One of the main purposes of the present analysis is to quantify the mechanical properties of contrast agent microbubbles. In this direction the analytical results from Reissner's theory [10] is a starting point. Reissner estimated the deformation of a spherical shell, when a *point* load is applied in one pole and then by minimizing the total elastic energy (balance between stretching and bending) near the pole he obtained a linear relation:

$$F = \frac{4}{\left[3(1-\nu^2)\right]^{0.5}} \frac{Eh^2}{R_o} \Delta \tag{13}$$

It should be stressed that as long the relation between the applied force (F) and the deformation (Δ) remains linear the deformed shape is flattened, e.g. no buckling has occurred. Thus, when the in-plane tensions become compressive, the shape buckles. With this reasoning, Pogorelov [11] described analytically the post-buckling force-deformation relation:

$$F = \left[\frac{3.56E^2h^5}{(1-\nu^2)^2 R_o^2} \Delta \right]^{0.5} \tag{14}$$

Coupling of equations (13) and (14) is a valid method for estimation of Young's modulus and shell thickness, especially for polymeric microbubbles [24]. The previous discussion on force-deformation regimes imply that, based on the above two stages, and combining the appropriate asymptotic relations we can predict the elastic properties of the shell. This approach was introduced in [24] and provided reliable estimates of the elastic properties of hard polymeric shells. Following and extending Reissner's work, we can estimate the force-deformation relation when a *flat and rigid punch* is in contact with a spherical shell:

$$F = \frac{4}{\sqrt{3\left(1-\nu^2\right)}}\frac{Eh^2\Delta}{R_o} + 0.06543\frac{Eh\Delta^2}{R_o} \tag{15}$$

The last expression has an additional term ($\sim\Delta^2$) comparing to equation (13), signifying the effect of *plane contact*. In this case the regime is called Stage I [25]. It represents a correction to the Reissner asymptotic prediction that holds until before buckling and crater formation take place. Increasing the external loading the spherical shell buckles forming an axisymmetric dimple (Stage II) and the force-deformation relation provided in eq (14) is recovered:

$$F = 3.807\frac{Eh^3}{\left(1-\nu^2\right)R_o}\left(\frac{\Delta\sqrt{1-\nu^2}}{h}\right)^{1/2} \tag{16}$$

In the following section an attempt is made to obtain parameter estimates for the microbubble coating based on the analysis leading to the correction of Reissner's formula, i.e. employing eq. (15).

As an alternative approach aiming at capturing the initial nonlinear part in the response curve, the effect of surface tension in f-d curves is investigated in the limit of small deformations by employing a balance of the associated energies near the contact area, before buckling takes place. In particular, following Shanahan's analysis for the appraisal of solid/solid interfacial interactions [8] when the particle subjected to external loading via AFM is a hollow elastic shell, we extend it in order to obtain estimates of the shell mechanical properties once the interfacial energy is known. Thus the different contributions to the cantilever/shell system read as follows.

Mechanical energy due to the displacement of the cantilever Δ, see also Figure 2, and the resulting deformation of the top of the shell:

$$G_M = -FR_0\Delta = -FR_0\left[\frac{\theta^2}{2} - \theta^4\left(\frac{1}{24}+\lambda\right)\right] \tag{17}$$

$$\Delta = R_0 - b = R_0 - R\cos\theta \xrightarrow{R-R_0=R_0\lambda\theta^4} \Delta/R_0 \approx \frac{\theta^2}{2}\left[1-2\theta^2\left(\frac{1}{24}+\lambda\right)+\ldots\right] \tag{18}$$

where $\lambda = \frac{1}{16}\frac{3(1-\nu)\tilde{P}}{2+3\left(1-\nu\right)\tilde{P}}$ from Shanahan's work [8] and is a measure of the resistance to compression of the microbubble in comparison with the resistance to stretching of the shell that surrounds it.

Energy associated with volume compression of the microbubble in the absence of prestress:

$$G_P \approx \theta^8\frac{K}{2}\left(3\lambda - \frac{3}{16}\right)^2, \quad K = \frac{4}{3}\pi R_0^3 P_A \tag{19}$$

Energy due to shell stretching at the contact area with the cantilever in the absence of any prestress:

$$G_E = \frac{Eh}{1-\nu}\oint_A e^2 dA \approx 4\pi\frac{Eh}{1-\nu}R_0^2\lambda^2\theta^8\left(1+2\lambda\theta^4\right) \tag{20}$$

where *e* represents deformation in the shell principal directions.

Energy due to interfacial forces (adhesive or repulsive) between the shell and the cantilever:

$$G_A = -\pi R_o^2\left(\theta^2 - \frac{\theta^4}{3}\right)W_s \tag{21}$$

with W_s representing surface energy between the shell the cantilever and the surrounding medium. In the present analysis the case of adhesion is presented in the interest of clarity. At equilibrium the energy minimization principle requires:

$$\frac{dG_T}{d\theta}=0\Rightarrow\frac{d\left(G_M+G_E+G_A+G_p\right)}{d\theta}=0\xrightarrow{\frac{\Delta}{R_o}\sim\frac{\theta^2}{2}\quad\text{and}\quad\frac{\Delta}{R_o}=d}$$
$$F\left[1-8d\left(\lambda+\frac{1}{24}\right)\right]-\frac{32\pi Eh\lambda^2R_o}{1-\nu}\left(8d^3+96\lambda d^5\right)-d^3\frac{6\pi R_0^2P_A}{\left(2+3(1-\nu)\tilde{P}\right)^2}+\left(2\pi R_oW_s-\frac{8\pi R_oW_sd}{3}\right)=0 \tag{22}$$

The last equation represents a force balance upon the cantilever at equilibrium consisting of the external load F and the different resistances that the external load has to overcome; the direction towards the interior of the shell is taken to be positive. In the limit of small deformations ($\theta\to0$), when adhesive forces prevail, a non-zero force ($F_o \sim -2\pi R_oW_s$) is required in order to overcome cantilever adhesion upon the shell and obtain zero deformation. Moreover, as the external load tends to positive values through zero, thus pushing the cantilever onto the shell, then the term due to elasticity and compression, $\sim \theta^6$, and the term due to surface tension $\sim \theta^0$, have to balance each other which means that for a particular range of elastic properties the adhesive forces can balance elasticity. If so, then

$$F_0=-2\pi R_0W_s$$
$$\frac{W_s\left(1-\nu\right)}{Eh}\approx\left(\frac{\Delta_0}{R_0}\right)^3\left[\frac{32\cdot4}{16^2}\left(\frac{3(1-\nu)\tilde{P}}{2+3(1-\nu)\tilde{P}}\right)^2+\frac{3(1-\nu)\tilde{P}}{\left[2+3(1-\nu)\tilde{P}\right]^2}\right],\qquad\left(\tilde{P}\equiv\frac{P_AR_0}{Eh}\right) \tag{23a,b}$$

In fact, the force balance described in eqs. (22) and (23a,b) may explain the initial nonlinear part in the response curve of soft shells, see also Figure 3 below, as it is for such shells that adhesion and elastic energy may be comparable, i.e. $W_s\left(1-\nu\right)\approx Eh$. Currently available data, e.g. fig 6 in [2] do not indicate the existence of a pull-off force, since phospholipids and silicon oxide forming the cantilever are both hydrophilic and repel each other. However, a similar analysis can be performed pertaining to repulsive forces by introducing the above mentioned interaction potential, W_s, corresponding to a disjoining pressure term at the interfacial stress balance between the shell and cantilever [9]. This allows for the existence of a wetting layer between the cantilever and the shell [9, 26]. Then, assuming fixed distance between the shell and cantilever, a positive force is required from the cantilever in order to balance the disjoining pressure and achieve zero displacement with the rest of the analysis remaining the same as for the case with adhesion.

It should also be pointed out that proper modelling of the adhesion of phospholipid shells onto nearby surfaces, e.g. inflammatory tissue, is essential for obtaining the acoustic signature of bound microbubbles that are employed for targeted drug delivery [27]. Depending on the interfacial energies of the involved media, the contact angle θ_w at very small contact areas based on the tangential balance eq. (10) will determine the adhesion force, $2\pi r_c\gamma_{BW}\sin\theta_w$. The tangential component is typically tensile [7] thus explaining the retardation of shell buckling and the advent of the Pogorelov regime. The above scenario constitutes a plausible conjecture that needs to be validated by experimental and numerical observations.

In this context, obtaining the pull-off force (F_o) in an AFM measurement, eq. (23a), may provide the adhesion energy W_s which subsequently, upon identifying the extent of contact θ_0 or the equivalent displacement Δ_0 in the

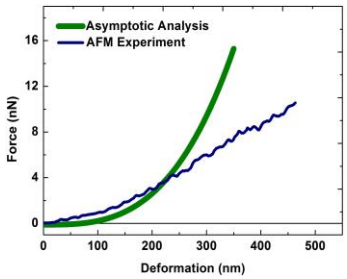

Figure 3. F~d plot of based on equation (22) against experimental [2] AFM data for a lipid microbubble with R_o=1.82 μm; χ=0.085 N/m; W_s=10^{-5} N/m

absence of any external forcing, can provide the area dilatation modulus $\chi=Eh$ via eq. (23b). It should be stressed that for such shells the thickness h is not a meaningful parameter. Rather, it is bending resistance that can be used as an independent parameter, however, in the context of the above analysis it is considered to be subdominant to adhesion or repulsion, stretching and pressure forces and does not appear in the force balance.

3 RESULTS

3.1 Parameter Estimation

Fitting the equation (15) from stage I in the linear part of the experimental f-d curve [3], it is possible to estimate the coefficients of Δ and Δ^2 for known initial radius (R_o) and ν=0.5. In the present study we employ this method as an alternative approach for parameter estimation to the one presented in [24] via combination of the Reissner and Pogorelov regimes, eq's (13, 14), in the response curve subject to a point load. For instance, in Figure 1(a), the experimental f-d curve of a polymeric microbubble with R_o=1.3 μm gives

$$\frac{4}{\sqrt{3\left(1-\nu^2\right)}}\frac{Eh^2}{R_o}=10 \text{ and } 0.06543\frac{Eh}{R_o}=1.6\cdot10^7 \Rightarrow E=20\cdot10^9\,\text{Pa and } h=16\cdot10^{-9}\,\text{nm} \tag{24}$$

which is in good agreement with the experimental estimation [3] of the same properties. It should also be stressed that in the experiments the shell thickness was estimated based on a linear equation [28] provided by the manufacturer and the Young's modulus from Reissner's equation (13). In Table 1, we compare the calculated values of the above properties via the experimental estimation [3] for microbubbles covered with polymeric biomaterial against the estimates provided by eq. (15) for a flat punch and those provided by the Reissner to Pogorelov transition for a point load, eqs (13, 14) from [24]. Both approaches exhibit satisfactory agreement with the experimental data in the estimated parameters, which supports the idea of applying the results of classical mechanics for characterizing such hard shells.

		Experimental Values [3]		Asymptotic Estimation Point Load		Asymptotic Estimation Plane Contact	
	D_o [μm]	E [GPa]	h [nm]	E [GPa]	h [nm]	E [GPa]	h [nm]
k_c=0.61 N/m							
	2.6	10-16	20	8.5	25	20	16
	3.5	4-8	26	12	26	5	30
	4.1	2.5-6	31	6.1	31	4.6	33
k_c=1.14 N/m							
	3.1	6-10	23	3.4	35	10	19
	3.2	6-10	24	14	20	6.7	27
	4.0	2.5-6	30	4.7	30	4.7	28
	4.9	1-3	37	4.5	31	4.9	28
	5.5	1-3	41	1.7	47	2	40

Table 1 : Comparison of elastic properties between experimental and asymptotic estimation for a polymeric shell

Preforming similar fitting calculations on an experimental AFM curve of a phospholipid microbubble [2], see also Figure 4(a), it is possible to estimate the Young's modulus and shell thickness in the same fashion as for polymeric shells. The calculated values using the flat punch approach, eq. (15), are E=80·MPa and h=9·nm which is in accordance with the experimental estimates, i.e. E=17 MPa and h=5 nm from [2]. Despite the agreement between calculation and experiment, the applicability of this approach for lipid shells is questionable as it is based on a correction to Reissner's theory and a balance between bending and stretching resistances, which is not expected to form the dominant balance for such soft coatings for which interfacial forces should be also accounted for.

3.2 Simulations

Based on the above parameter estimates simulations were performed using the numerical methodology described in section 2.2 for the response to a point load, and Abaqus for simulating the response to a flat punch. The force-deformation curve pertaining to the response of a polymeric shell to a point load is plotted against the

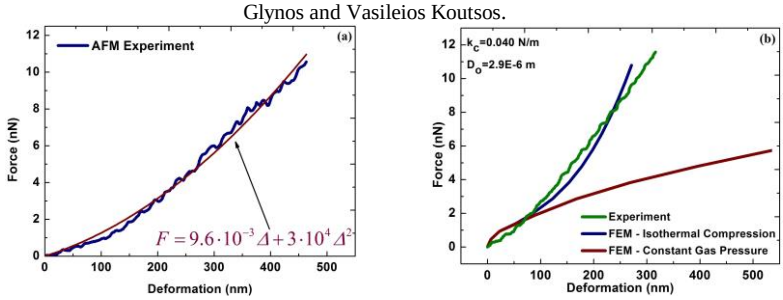

Figure 4. (a) Asymptotic fitting in f-d curve for a lipid microbubble [2], (b) Comparison between experimental [2] and FEM results for a microbubble covered with phospholipid

experimental data for the estimated elastic properties of Table I in Figure 1(b). The calculated curve has an initial linear regime, which is followed by a nonlinear one recovering the transition from Reissner to Pogorelov regime. It should be stressed that the simulation curve exhibits a faster transition to Pogorelov regime, which is associated with the point load approximation and the estimation of deformation exactly at θ=0 [24]. In Figure 4(b) the experimental curve is compared against the finite element results for microbubbles covered with phospholipids that are subject to a point load. The numerical curve (blue curve) verifies transition from Reissner to Pogorelov, but for a small range of deformations. An additional fourth regime dominates the f-d curve at large deformations, which is associated with gas compressibility. Another simulation with constant internal pressure results in an f-d (red) curve with identical transition from Reissner to Pogorelov but without the curved upwards regime dominated by gas compressibility. In fact, the dimensionless numbers (eq. 8) that correspond to the mechanical properties employed in the simulations provide insight regarding the dominant forces that balance the external applied load:

$$\text{Polymer: } \tilde{k}_b = 4 \cdot 10^{-5},\ \tilde{P} = 6 \cdot 10^{-4} \quad ; \quad \text{Phospholipid: } \tilde{k}_b = 7 \cdot 10^{-6},\ \tilde{P} = 3.4 \cdot 10^{-1} \tag{25}$$

As the dimensionless bending modulus increases bending resistance grows and the buckling of the spherical shell is shifted to higher values. Moreover, for the case of a phospholipid shell the dimensionless pressure is quite large indicating that the gas compressibility is comparable with elasticity, thus constituting an important additional stiffness that the external load has to balance.

Upon performing Abaqus simulations for a microbubble coated with an elastic shell in contact with a plane and rigid cantilever, we have produced universal force-deformation curves, Figure 5(a), for fixed shell thickness to radius ratio (R/h=100). In particular, the simulation shows that initially the force deformation curve is curved upwards indicating an increase of shell stiffness. This response obtained for the parameters pertaining to a polymeric shell, Figure 1(a), is associated with stage I as discussed in the previous section. Increasing the external load the response changes and the force-deformation curve is curved downwards indicating buckling of the shell and crater formation in the vicinity of the pole that is subjected to the flat cantilever, stage II, while in stage I the contact area is flattened. In addition, the cantilever displacement is plotted against the deformation of the shell, showing that as long the shell is flattened both displacements are equal, but when the shell buckles the shell displacement has a delay in comparison with the point load, Figs. 6(a,b).

However, once the parameters that were estimated based on the correction to Reissner's theory by asymptotic relation eq. (15) are employed in order to simulate the f-d curve for a phospholipid shell, Figure 4(a), buckling and transition to crater formation are predicted for an unrealistic value of the external force, Figure 5(b). This is attributed to the fact that for such soft shells intermolecular forces are required for properly simulating the response at small deformations, whereas such forces are not included in the correction to Reissner eq. (15). More simulations are required in order to provide insight on the effect of intermolecular forces on the f-d curve. The increase of intermolecular forces has an impact on the transition from stage I to stage II. In particular, as the control parameter f that represents a point shear load at the edge of contact between the cantilever and the shell increases, buckling occurs for higher values of deformation whereas for very large values the shell never buckles. This is a result of the point shear load counteracting the shear that develops on the shell as a result of bending at the edge of contact. Including adhesion forces in the model is expected to provide an additional force that pushes the shell against the cantilever along with a shear force that depending on the contact angle, see also Figure 2(c) and eq's (10-11), postpones buckling. A preliminary estimate of the impact of surface adhesion on the response is provided in Figure 3 for a microbubble of radius R_0=1.82 μm with shell modulus χ=0.085 N/m and interfacial energy W_s=10^{-5} N/m , that qualitatively illustrates the impact of adhesion at small displacements and its potential in capturing the initial nonlinear regime in f-d curves. In particular, as the shell stiffness increases in comparison with surface energy the shell response at small deformations for loads on the order of nN, acquires the relatively

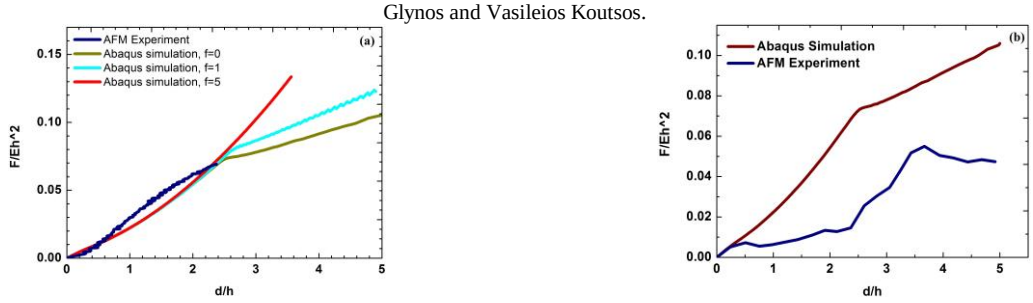

Figure 5. Force-deformation curves obtained with Abaqus against experimental data for (a) a polymeric microbubble (R_o=1.3 μm; χ=212 N/m) [3] and (b) a phospholipid shell (R_o=1.82 μm; χ=0.085 N/m) [2]

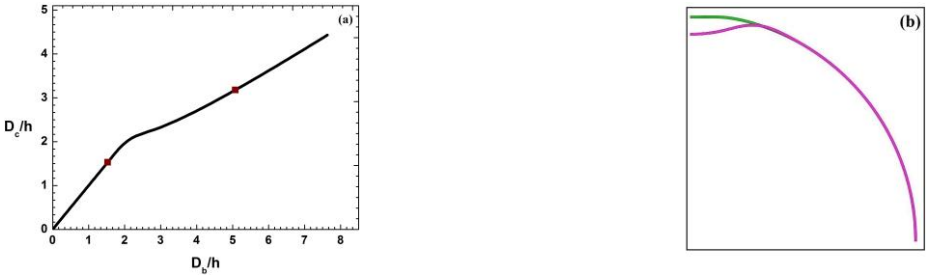

Figure 6.(a) Cantilever displacement versus shell displacement and (b) Microbubble in deformed configuration for d/h=1.5 and 5, corresponding on red dots of (a), both for a polymeric microbubble.

flat nonlinear profile often exhibited by statically interrogated shells before the classic linear response pattern sets in.

4 CONCLUSIONS

The response of microbubbles that are coated with a polymeric shell, subject to a static load, was investigated numerically and the results are compared against experimental data [2, 3]. The Young's modulus along with the thickness of the shell can be easily estimated from f-d curves by fitting the linear and nonlinear regimes with the asymptotic relations from Reissner's and Pogorelov's theory. An extension of Reissner and Pogorelov theory is discussed in the present work in order to include the effect of plane contact instead of point forcing. The analytical form of Reissner and Pogorelov extension can also accurately estimate the above properties. The results of both approximations are in accordance with the relevant experimental values, proving that in analogous experiments the shell thickness need not be a-priori known. In particular, knowledge of the force and deformation pertaining to the buckling point signifying transition from flat to dimpled shell during AFM measurements provides enough information for the estimation of the elasticity modulus and shell thickness. Numerical studies of the contact problem between an elastic shell and a rigid plate verify this assertion [29]. This can be a very useful tool in AFM studies aiming at the mechanical characterization of coated microbubbles, especially the ones with polymeric shells whose small size and preparation procedures do not allow for reliable estimates of their shell thickness, as long as the available AFM apparatus allows for visual or other identification of the onset of buckling and crater formation.

Numerical simulations with the finite element method, employing the elastic parameter values estimated by treating the experimental f-d curves in the above fashion, confirm the transition from Reissner to Pogorelov regime, but exhibit discrepancies with equivalent experimental f-d curves. These discrepancies are attributed to the point force which accelerates transition to the Pogorelov regime (or buckling stage) and the fact that no surface forces are included in the present FEM model. Adding these parameters in the modeling is expected to provide more reliable results. Simulations with Abaqus indicate that buckling is affected by surface forces. In particular, as the surface forces increase buckling occurs for higher values of deformation. Identifying the nature of surface forces is an essential element for parameter characterization.

In the case of phospholipid shells verifying via careful measurements the existence of a small but non-zero force required for zero displacement, while registering the f-d curve at small displacements, is expected to provide an alternative means for estimating the area dilatation modulus of soft shells from the initial nonlinear part of their response curve. Simulations are currently performed in order to integrate the above regimes in the response curve of phospholipid shells whose soft shell allows for interfacial forces to play a key role in the force balance for external loads on the order of nN.

5 ACKNOWLEDGMENTS

This work is performed in the framework of the operational program: «Education and lifelong learning» - «Aristeia» and is cofounded by the European Union (European Social Fund) and national resources.

REFERENCES

[1] Ferrara, K., Pollard, R., Borden, M., (2007), "Ultrasound microbubble contrast agents: Fundamentals and application to gene and drug delivery", *Annual Review Biomedical Engineering*, Vol. 9, pp. 415-447.

[2] Buchner Santos, E., Morris, J., Glynos, E., Sboros, V., Koutsos, V., (2012), "Nanomechanical properties of phospholipid microbubbles", *Langmuir*, Vol. 28, pp. 5753-5760.

[3] Glynos, E. et al., (2009), "Nanomechanics of biocompatible hollow thin-shell polymer microspheres", *Langmuir*, Vol. 25, pp. 7514-7522.

[4] Glynos, E., Sboros, V., Koutsos, V., (2009), "Polymeric thin shells: Measurement of elastic properties at the nanometer scale using atomic force microscopy", *Mat. Sci. and Eng. B*, Vol. 165, pp. 231-234.

[5] Stride, E., Saffari, N., (2003), "Microbubble ultrasound contrast agent: a review", *Proceedings of the Institution of Mechanical Engineering*, Vol 217, Part H: Journal of Engineering in Medicine, pp. 429-447.

[6] Liu, Y., Miyoshi, H., Nakamura, M., (2006), "Encapsulated ultrasound microbubbles: Therapeutic application in drug/gene delivery", *Journal of Controlled Released*, Vol. 114, pp. 89-99.

[7] Johnson, K., Kendall, K., Roberts, A., (1971), "Surface energy and the contact of elastic solids", *Proceedings of the Royal Society of London A*, Vol. 324, pp. 301-313.

[8] Shanahan, M., (1997), "A novel test for the appraisal of solid/solid interfacial interactions", *Journal of Adhesion*, Vol. 63, pp. 15-29.

[9] Israelachvili, J.N., (2011), *Intermolecular and surface forces*, Elsevier, USA.

[10] Reissner, E., (1946), "Stresses and small displacements of shallow spherical shells I and II", *Journal of Mathematical Physics*, Vol. 25, pp. 279-300.

[11] Pogorelov, A., (1988), *Bendings of surfaces and stability of shells*, American Mathematical Society, USA.

[12] Vella, D., Ajdari, A., Boudaoud, A., (2011), "Wrinkling of pressurized elastic shells", *Physical Review Letters*, Vol. 107, pp. 174301.

[13] Lytra, A., Pelekasis, N., (2014), "Static response and stability of coated microbubbles—multiplicity of solutions and parameter estimation", *Fluid Dynamics Research*, Vol. 46, pp. 041422.

[14] Weatherburn, C.E., (1955), *Differential geometry of three dimensions*, Cambridge University Press.

[15] Timoshenko, S., Woinowsky-Krieger, S., (1959), *Theory of plates and shells*, McGraw-Hill.

[16] Libai, A., Simmonds, J., (2005), *The nonlinear theory of elastic shells*, Cambridge University Press.

[17] Pozrikidis, C., (2001), "Effect of membrane bending stiffness on the deformation of capsules in simple shear flow", *Journal of Fluid Mechanics*, Vol. 440, pp. 269-291.

[18] Tsiglifis, K., Pelekasis, N., (2011), "Parametric stability and dynamic buckling of an encapsulated microbubble subject to acoustic disturbances", *Physics of Fluids (1994-present)*, Vol. 23, pp. 012102.

[19] Barthes-Biesel, D., Diaz, A., Dhenin, E., (2002), "Effect of constitutive laws for two-dimensional membranes on flow-induced capsule deformation", *Journal of Fluid Mechanics*, Vol. 460, pp. 211-222.

[20] Landau L.D., Lifshitz, E.M., (1986), *Theory of Elasticity*, Elsevier, Butterworth-Heinemann, Oxford.

[21] Prenter, P.M., (1989), *Splines and Variational Methods*, Wiley, USA.

[22] Boor, C. de, (2001), *A practical guide to splines*, Springer, USA.

[23] Pelekasis, N., Tsamopoulos, J., Manolis, G., (1990), "Equilibrium shapes and stability of charged and conducting drops", *Physics of Fluids A*, Vol. 2, pp. 1328-1340.

[24] Lytra, A., Pelekasis, N., Sboros, V., Glynos, E., Koutsos, V., "Static response of coated microbubbles: Modeling simulations and parameter estimation", accepted article in *Procedia IUTAM*.

[25] Vasiri, A., (2009), "Mechanics of highly deformed elastic shells", *Thin-Walled Structures*, Vol. 47, pp. 692-700.

[26] Blount, M., Miskis, M., and Davis, S., (2015) "The equilibria of vesicles adhered to substrates by short ranged potentials", *Proceedings of Royal Society A*: 469 2012.0729.

[27] Sboros, V., et al., (2010) "Probing microbubble targeting with atomic force microscopy" *Colloids and Surfaces B: Biointerfaces*, Vol. 80, pp. 12–17.

[28] Ottoboni, T., et al., (2004), "Hollow microspheres with controlled fragility for medical use", US 6776761B2.

[29] Updike, D.P., Kalnins, A., (1972), "Contact pressure between an elastic spherical shell and a rigid plate", *Journal of Applied Mechanics*, Vol. 39, pp. 1110-1114.